J Mater Sci (2008) 43:132–138
DOI 10.1007/s10853-007-2123-7

Mechanochemical behavior of Fe_2O_3–Al–Fe powder mixtures to produce Fe_3Al–Al_2O_3 nanocomposite powder

M. Khodaei · M. H. Enayati · F. Karimzadeh

Received: 31 March 2007 / Accepted: 21 August 2007 / Published online: 29 September 2007
© Springer Science+Business Media, LLC 2007

Abstract Mechanical treatment of Fe_2O_3, Al and Fe powder mixtures was carried out in a high energy ball mill to synthesize Fe_3Al–Al_2O_3 intermetallic matrix nanocomposite. Different compositions including 3Fe + Al, Fe_2O_3 + 2Al, $3Fe_2O_3$ + 8Al and Fe_2O_3 + 3Al+Fe were chosen in this study. Phase development and structural changes occurring during ball milling were investigated by X-ray diffractometry (XRD) and scanning electron microscopy (SEM). The results showed that during MA, Fe_2O_3, Al, and Fe react to give a nanocrystalline Fe_3Al intermetallic compound matrix. The presence of pure Fe in initial powder mixture changed the modality of mechanochemical process from sudden to gradual reaction. The Fe_3Al–Al_2O_3 compound had a finer microstructure and particles size compared to the Fe_3Al compound.

Introduction

Fe_3Al intermetallic compound is an important class of materials, due to a combination of its high tensile strength, low density, good wear resistance, ease of fabrication, and low cost. It also has excellent oxidation, sulfidation, and corrosion resistance at high temperature. These properties have led to the identification of several potential usages including structural applications and protective coatings [1–4]. Two major problems that restrict the application of Fe_3Al are poor low-temperature ductility and inadequate high-temperature creep resistance. These limitations can be overcome by introducing ceramic particles as reinforcements [5]. Reinforcement phase can be produced by in-situ techniques such as a mechanochemical process using displacement reactions. Various nanocomposites including Cu–Al_2O_3 [6], Ni–Al_2O_3 [7], NiAl–Al_2O_3 [8], and FeAl–Al_2O_3 [9], have been successfully produced by mechanochemical synthesis route. Mechanochemical technique has an advantage over other processing methods as it is capable of producing nanometer reinforcement particles in the matrix with high uniformity [10].

In this work, the fabrication of Fe_3Al-30 vol.% Al_2O_3 nanocomposite powder by ball milling of elemental powders (Fe_2O_3, Al, and Fe) is investigated. Details of the processing steps, kinetics consideration, phase development and microstructural characterizations are also discussed.

Experimental methods

The raw materials were Fe (–300 μm, 99.5% purity, water atomized), Al (–100 μm, 99.5% purity, water atomized), and Fe_2O_3 (–5 μm, 99.99% purity, reagent grade, Merck product). Mechanical treatment was performed in a Spex8000 type ball mill. The milling media consisted of five 12 mm diameter balls, confined in a 75 mL volume vial. The ball and bowl materials were hardened chromium steel. In all milling runs, the ball-to-powder weight ratio was 5:1, and the vial rotation speed and vibration frequency were 700 rpm and 11.7 Hz, respectively. A total of 7 g powder with no process control agent was milled under argon atmosphere to avoid oxidation. The phase changes that occurred during ball milling were investigated by X-ray diffraction analysis using a Philips X'PERT MPD diffractometer with CuKα radiation (λ = 0.15405 nm).

M. Khodaei · M. H. Enayati (✉) · F. Karimzadeh
Department of Materials Engineering, Isfahan University of Technology, Isfahan 84156-83111, Iran
e-mail: ena78@cc.iut.ac.ir

X-ray diffraction was performed with a 0.03 step and counting time of 1 s per point. Crystallite size and mean lattice strain (estimated by the Williamson–Hall method [11]) were calculated from the XRD patterns. Morphology and cross-sectional microstructure of powder particles were examined by scanning electron microscopy (SEM) using a Philips XL30 microscope. Differential thermal analysis (DTA) was carried out in a PL-STA1640 thermal analyzer under flowing argon atmosphere in alumina crucibles, within a temperature range of 30–1000 °C, applying a heating rate of 15 °C/min.

Results and discussion

The formation of Fe_3Al and Al_2O_3 phases during ball milling was investigated by choosing four different systems as listed in Table 1.

Formation of Fe_3Al

Ball milling of elemental Fe and Al powder mixture with composition $Fe_{75}Al_{25}$ was carried out in order to investigate the formation mechanism of the Fe_3Al during ball milling according to reaction 1.

$$3Fe + Al = Fe_3Al \quad \Delta H = -66.9 \text{ kJ/molK} \tag{1}$$

XRD patterns of starting powder as-received and after different milling times are presented in Fig. 1. Diffraction lines of as-received powder mixture show the XRD peaks of Fe and Al, in which (200), (220), and (222) peaks of Al are superimposed on (110), (200), and (211) peaks of Fe. Only (111) and (311) peaks of Al are unaffected. After 5 h of milling time, the intensity of all XRD lines decreased. The disappearance of Al peaks in the early stage of ball milling indicates that the aluminum particles are scrappy, and conceivably situated into the grain boundary of iron [12]. As seen in Fig. 1, the positions of Fe and Al diffraction lines, after 5 h of milling time, did not change. After 10 h of milling time, the (111) and (311) peaks of Al virtually vanish, and the other peaks are broadened suggesting the refinement of grain size, and increasing

Table 1 Different reactions among Fe_2O_3, Al and Fe powder mixtures studied here

Reactions	Products
3Fe + Al	Fe_3Al
Fe_2O_3 + 2Al	Fe + 64 vol.%. Al_2O_3
$3Fe_2O_3$ + 8Al	Fe_3Al + 57 vol.% Al_2O_3
Fe_2O_3 + 3Al + Fe	Fe_3Al + 30 vol.% Al_2O_3

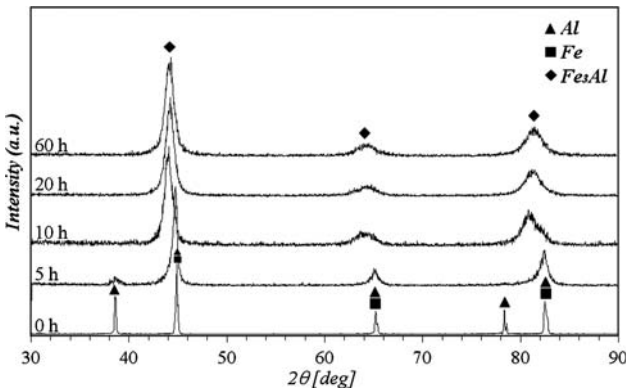

Fig. 1 XRD patterns of 3Fe + Al as-received and after different milling times

the level of lattice strain. It should be noted that XRD peaks after 10 h of milling time are asymmetric and the extra broadening of these peaks is due to the presence of two neighboring peaks. All peaks have two distinctive diffraction lines (Fe(Al) solid solution and Fe). XRD patterns of 20 h milled powders show three peaks, which were identified as a bcc-Fe(Al) solid solution (disordered Fe_3Al intermetallic compound). Increasing the milling time to 60 h had no obvious effect on the XRD patterns.

Figure 2 shows the cross-sectional images of $Fe_{75}Al_{25}$ powder particles after 3 and 5 h of milling times. In the early stage of milling, a lamellar structure of elemental Fe and Al was formed in agreement with XRD results. Repeated cold welding and fragmentation decrease the interlamellar spacing at longer milling times as shown in Fig. 2b.

The results of SEM observations and XRD analysis show that the elemental powders remain elemental in lamellar structure in the early stage of milling, and then transformed directly to the Fe_3Al intermetallic compound, with nanocrystalline structure at longer milling time. This phenomenon has previously been investigated [13].

Mechanochemical reaction of Fe_2O_3 + 2Al

Figure 3 shows the XRD patterns of Fe_2O_3 and Al powder mixture with stoichiometric composition as-received, and after different milling times. The reaction between Fe_2O_3 and Al powders occurred during ball milling according to the following reaction:

$$Fe_2O_3 + 2Al = 2Fe + Al_2O_3 \quad \Delta H = -851.6 \text{ kJ/molK} \tag{2}$$

The volume fraction of Al_2O_3 produced by the stoichiometric reaction is about 64%. The formation of Fe and

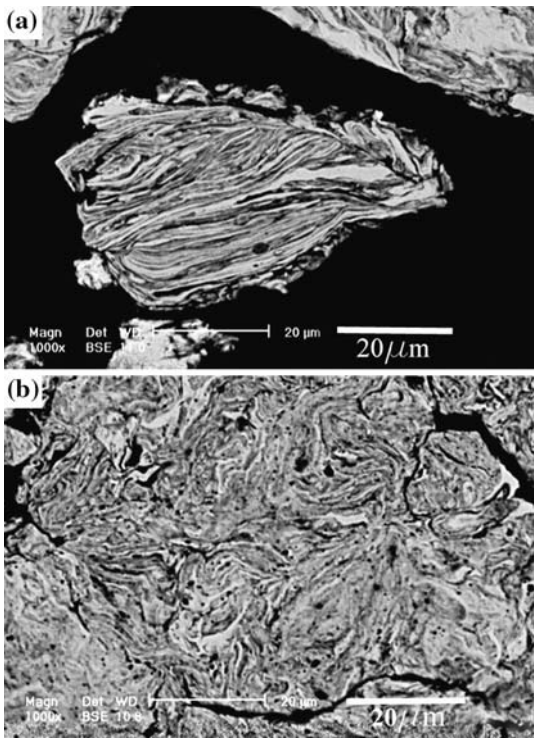

Fig. 2 Cross-sectional SEM images of 3Fe + Al powder particles after (**a**) 3 h and (**b**) 5 h of milling times

Al_2O_3 appeared to be completed after 3 h of milling. The diffraction lines of reaction products were identified as bcc-Fe and α-Al_2O_3 phases. No considerable dissolution of Al in Fe was observed. In contrast, Matteazzi et al. reported that an Fe(Al) solid solution containing 1.7 at.% Al is formed during ball milling of Fe_2O_3 with Al [14]. As seen in Fig. 3, increasing the milling time up to 6 h did not affect the peak positions, but led to the broadening of Bragg peaks indicating the refinements of Fe and Al_2O_3 crystallite size, and the enhancement of lattice strain. The crystallite size and mean lattice strain of Al_2O_3 after 3 h of milling time were 77 nm and 0.62%, respectively, which changed to 28 nm and 0.75% after 6 h of milling time.

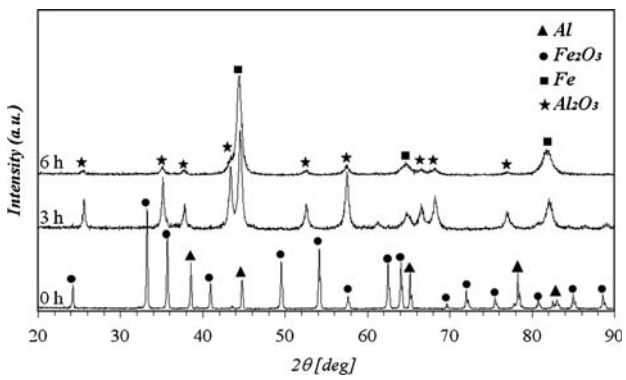

Fig. 3 XRD patterns of Fe_2O_3 + 2Al as-received and after different milling times

Reduction of Fe_2O_3 by Al [14, 15], Mg [15, 16], Ti [17], and H_2 [18] using high-energy ball milling has been previously reported. All these reactions have a large negative free energy change, and therefore, are thermodynamically feasible at ambient temperature. The only limitation for the occurrence of these reactions at low temperature is kinetic consideration.

The kinetics of solid state chemical reactions are ordinarily limited by the rate at which reactant species are able to diffuse across phase boundary, and through intervening product layers [19]. The underlying mechanism of reactive milling is repeated deformation, fracture, and cold welding of powder particles during collision of the grinding media. During ball milling of Fe_2O_3–Al powder mixture, the Fe_2O_3 particles are expected to disperse through the ductile reductant (Al) in a "current bun" [20] morphology. Chemical reaction during ball milling occurs either gradually or suddenly by mechanically activated combustion [19]. The modality of displacement reactions can be specified by T_{ad}. A value of $T_{ad} > 1{,}800$ K is generally considered to be the minimum necessary temperature for the occurrence of self-propagating combustion in a thermally ignited system [21]. In contrast, Schaffer and McCormick [22] showed that a value of $T_{ad} > 1{,}300$ K is adequate for the sudden occurrence of displacement reaction during ball milling. The T_{ad} value could be estimated from the following relation:

$$\Delta H_r + \sum \int_{T_i}^{T_m} {}^{s}C_p + \sum \Delta H_t + \sum \int_{T_m}^{T_{ad}} {}^{l}C_p = 0 \qquad (3)$$

where ΔH_r is the heat of reaction, T_i is the initial temperature, the T_ms are the melting points of products, the ${}^{s}C_p$s are the molar heat capacities of the solid products, ΔH_ts are the heat of transitions of the products and ${}^{l}C_p$s are the molar heat capacities of the liquid products. It should be noted that the last term in reaction 3 is ignored if $T_{ad} < T_m$s.

The value of T_{ad} for reaction 2, calculated using relation 3, is 3,398 K. Therefore, reaction in Fe_2O_3 + 2Al system can take place by combustive mode during ball milling. According to the XRD results, the reaction of Fe_2O_3 and Al was completed before 3 h of milling time. It is proposed that the ignition temperature decreases with increasing milling time as a result of microstructure refinement, mechanical activation, and the momentary temperature rise resulting from milling media collisions [19]. The local heat generation can lead to the formation of crystalline Al_2O_3 rather than the amorphous Al_2O_3.

Mechanochemical reaction of $3Fe_2O_3 + 8Al$

Figure 4 shows the XRD patterns of Fe_2O_3 and Al powder mixture as-received, and after 20 h of milling time according to the following reaction:

$$3Fe_2O_3 + 8Al = 2Fe_3Al + 3Al_2O_3 \quad \Delta H = -2688.6 \text{ kJ/molK} \tag{4}$$

The end-products of reaction 4 were identified as bcc-Fe_3Al and crystalline α-Al_2O_3. Fan et al. reported [23] that during reaction of Fe_2O_3 and molten aluminum, instead of thermodynamically predicted Fe_3Al intermetallic compound, $FeAl_2O_4$ is predominately formed. This is due to simultaneous formation of Fe_3Al and Al_2O_3, when the low diffusion rate of aluminum into $FeAl_2O_4$ controls the products of reaction. On the other hand, during solid state reaction of Fe_2O_3 and Al (as mentioned above), the formation of Fe_3Al does not occur in the early stage of milling. In the initial stage of ball milling, the Fe_2O_3 is first reduced to bcc-Fe by Al forming the α-Al_2O_3 phase. In the second stage, increasing the milling time resulted in the formation of Fe_3Al by the interdiffusion of Fe obtained from the first stage, and excess Al. Therefore, reaction 4 can be written as the following reaction:

$$3Fe_2O_3 + 8Al = 6Fe + 2Al + 3Al_2O_3 \quad \Delta H = -2554.8 \text{ kJ/molK} \tag{5}$$

The value of T_{ad} for reaction 5, calculated using relation 3, is 3,158 K indicating that the combustion reaction can take place in this system. α-Al_2O_3 forms suddenly, and whole of Fe_2O_3 is reduced completely during combustive reaction. The local heat generation leads to the formation of crystalline α-Al_2O_3 instead of amorphous Al_2O_3. The value of T_{ad} for reactions 2 and 5 is similar, and it can be assumed that the formation of Fe and Al_2O_3 in reaction 5 is similar to that in reaction 2. Thus, after a short time of milling (about 3 h) Fe, Al_2O_3, and the remaining Al coexist in the milling media, and further milling for 20 h leads to the formation of Fe_3Al phase as seen in Fig. 4. Volume fraction of produced Al_2O_3 according to reaction 4, is about 57%.

Mechanochemical reaction of $Fe_2O_3 + 3Al + Fe$

In order to obtain Fe_3Al–Al_2O_3 composite with lower volume fraction of Al_2O_3 (30 vol.%), elemental Fe was added to the starting materials according to the following reaction:

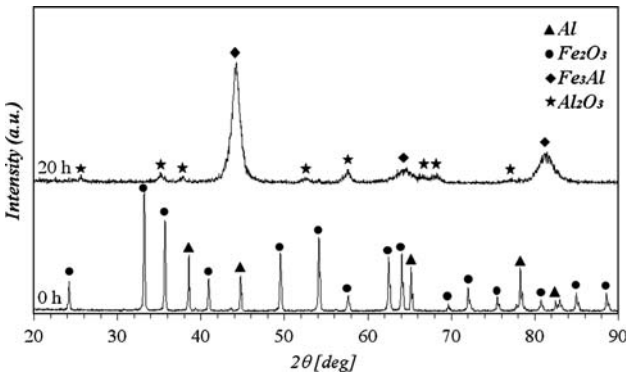

Fig. 4 XRD patterns of $3Fe_2O_3 + 8Al$ as-received and after 20 h of milling time

$$Fe_2O_3 + 3Al + Fe = Fe_3Al + Al_2O_3 \quad \Delta H = -918.5 \text{ kJ/molK} \tag{6}$$

XRD patterns of powder particles after different times of ball milling are presented in Fig. 5. The reactant powders at the initial time were α-Fe_2O_3, Fe, and Al, according to reaction 5 (calculated for 30 vol.%. Al_2O_3). The XRD patterns of milled powders after 3 and 6 h of milling times show the XRD peaks of as-received powders. Increasing milling time led to the broadening of the diffraction lines, as a result of refinement of crystallite size and an increase in the level of internal strain. As seen, addition of elemental Fe to the mixture of Fe_2O_3 and Al increases the start time of Fe_2O_3–Al solid state reaction. The T_{ad} is a measure of the local heat generated by the reaction, and since reaction rate increases with increasing temperature, it can have a significant effect on the reaction rate [19]. As mentioned above, the reaction 6 can be considered as follows:

$$Fe_2O_3 + 3Al + Fe = 3Fe + Al + Al_2O_3 \quad \Delta H = -851.6 \text{ kJ/molK} \tag{7}$$

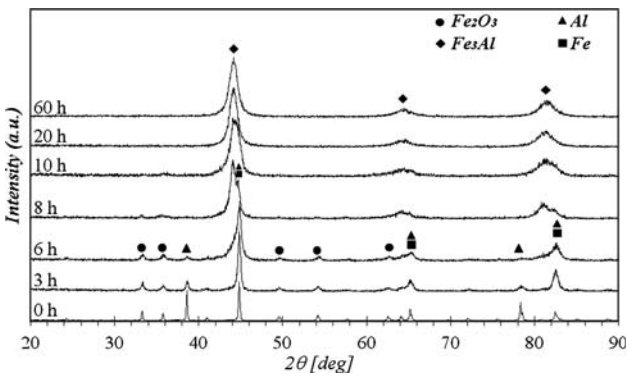

Fig. 5 XRD patterns of $Fe_2O_3 + 3Al + Fe$ as-received and after different milling times

The value of T_{ad} for reaction 7, calculated using relation 2, is about 725 K which is much lower than 1,300 K due to the dilution effect of excess Fe, which separates the reactants and suppresses the combustion reaction. Also, it was evidently shown [22] that during mechanical milling, there is a general increase in the precombustion period with a decrease in adiabatic temperature. Thus, the combustion reaction during solid state mechanochemical process is put off to the longer time as T_{ad} decreases. The kinetics of such a diluted system is controlled not only by diffusion rates but also by particles' size and reactant contact area in lamellar structure.

After 8 h of milling time, the Fe(Al) solid solution (disordered Fe_3Al intermetallic) forms partially coexist with as-received powders. After 10 h of milling time, the diffraction lines of Fe_2O_3 vanished, and three asymmetric peaks appeared. The XRD traces at this stage were identified as elemental Fe and Al along with Fe_3Al phases. Reduction of Fe_2O_3 occurs gradually, and the kinetics of this reaction depends on random contact of reactants, which controls the diffusion rate of displacement reaction. After 20 h of milling time, three symmetric peaks are formed, and we should emphasize that the peaks of Fe_3Al disordered intermetallic compound are formed completely. The Bragg peaks of Al_2O_3 are not seen in Fig. 5. The absence of peaks is due to the low volume fraction of Al_2O_3 and X-ray absorption by the Fe_3Al matrix. This effect was discussed using the phenomenon that is developed by Leonard and Koch [24]. The mass absorption coefficient of Fe_3Al (269.2 cm^2/g [25]) is very large compared to Al_2O_3 (31.7 cm^2/g [25]). As a result, the Al_2O_3 peaks will be suppressed by Fe_3Al-matrix absorption. Additionally, the refinement of Al_2O_3 to nanometer size causes the remarkable broadening of XRD peaks and a decrease in their intensity.

Figure 6 displays the SEM cross-sectional images of powder mixture (Fe_2O_3, Al, and Fe) after 3, 8, and 20 h of milling times. In agreement with XRD patterns, the cross-sectional images of powders after 3 and 8 h of milling times, demonstrate the existence of initial materials in powder particles. Fe_2O_3 particles are embedded in the lamellar structure of Fe and Al. Cross-sectional image of powder particles after 8 h of milling time, additionally shows some regions containing Fe_3Al phase in consistence with the XRD results. At the beginning of the process, the ductile powders (Fe and Al) get flattened by milling media collisions, while the brittle particles (Fe_2O_3) get fragmented and comminuted. The presence of excess Fe particles in the lamellar structure leads to the formation of a coarse Fe–Al structure. In this stage, further fragmentation and partitioning is required to space Fe_2O_3 particles closely along the interlamellar spacing of Al. The cross-sectional image of powder particles after 20 h of milling time, shows no lamellar structure indicating the complete formation of Fe_3Al phase.

The influence of Al_2O_3 on crystallite size and mean lattice strain of Fe_3Al phase was studied by Williamson–Hall approach. The X-ray diffraction pattern of 60 h milled Fe_3Al and Fe_3Al-30 vol.% Al_2O_3 are collected from 20 to 105° (Fig. 7) to use the diffraction peak of (220) in Williamson–Hall plots. Figure 8 shows the Williamson–Hall plots of these samples, in which only three points related to (110), (211) and (220) planes have lain approximately on straight lines. It should be noted that the point related to (200) plane is not in accordance with others due to the anisotropy in elastic properties of bcc-Fe(Al), analogical to Fe single crystal. The elastic module along [110] direction of bcc-Fe(Al) is low, and the strain along [110] direction (perpendicular to (200) plane) is much higher

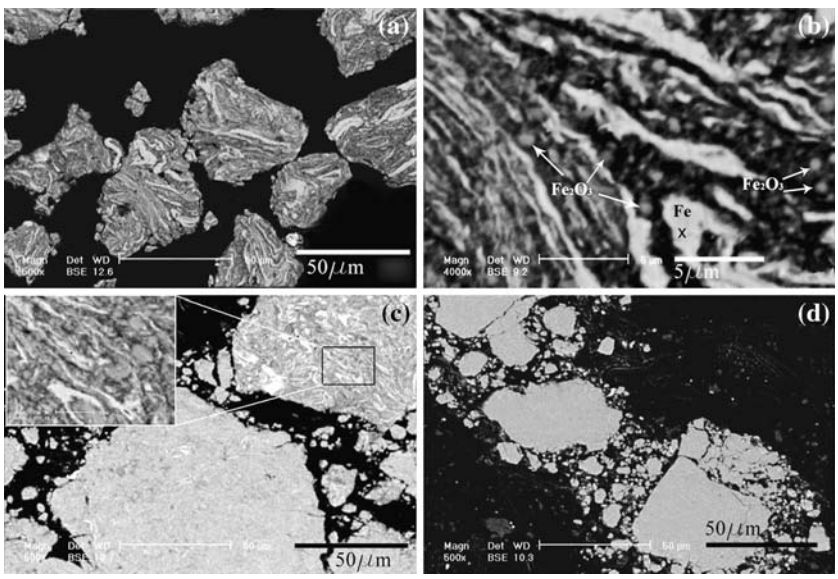

Fig. 6 Cross-sectional SEM images of Fe_2O_3 + 3Al + Fe powder particles after (**a**) and (**b**) 3 h, (**c**) 8 h and (**d**) 20 h of milling times

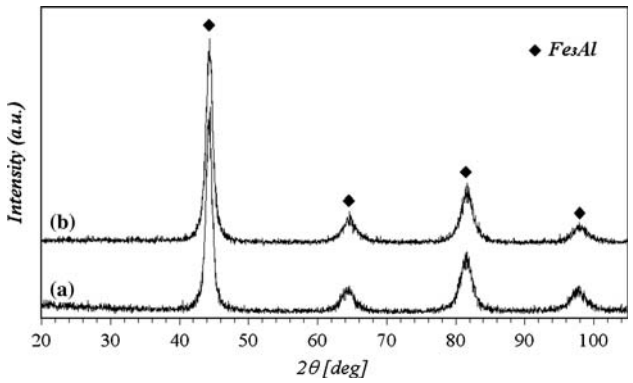

Fig. 7 XRD patterns of (**a**) 3Fe + Al and (**b**) Fe_2O_3 + 3Al + Fe after 60 h of milling time

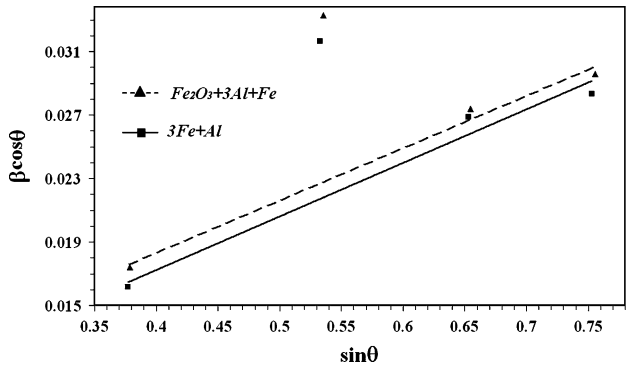

Fig. 8 Williamson–Hall plots for 3Fe + Al (Fe_3Al) and Fe_2O_3 + 3Al + Fe (Fe_3Al-30 vol.% Al_2O_3) after 60 h of milling time

after plastic deformation during ball milling. This leads to the extra broadening of (200) diffraction peak, and should not be taken into account. Crystallite size and mean lattice strain of Fe_3Al disordered intermetallic compound, with and without Al_2O_3, after 60 h of milling time are listed in Table 2. Presence of Al_2O_3 leads to a decrease in the crystallite size.

Figure 9 shows the morphology and powder particle size of Fe_3Al and Fe_3Al-30 vol.% Al_2O_3 after 60 h of milling time. As seen for both compositions, powder particles are irregular in shape, and the presence of in situ formed Al_2O_3 leads to a decrease in particle size.

The DTA curve of Fe_2O_3 + 3Al + Fe powder mixture, according to reaction 6, after 3 and 20 h of milling times are shown in Fig. 10. After 3 h, the DTA curve shows two

Table 2 Crystallite size, D, and lattice strain, ε, of 3Fe + Al (Fe_3Al) and Fe_2O_3 + 3Al + Fe (Fe_3Al-30 vol.% Al_2O_3) after 60 h of milling time

Sample	D (nm)	ε (%)
3Fe + Al	37	1.65
Fe_2O_3 + 3Al + Fe	28	1.69

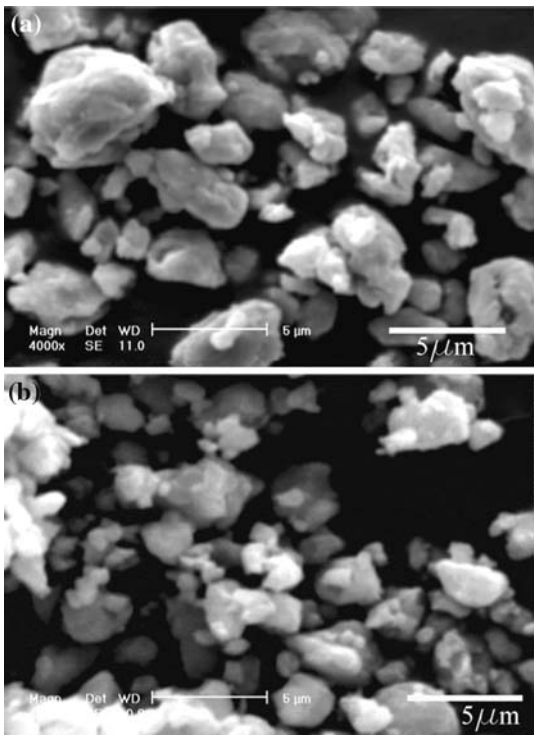

Fig. 9 SEM images of (**a**) 3Fe + Al (Fe_3Al) and (**b**) Fe_2O_3 + 3Al + Fe (Fe_3Al-30 vol.% Al_2O_3) after 60 h of milling time

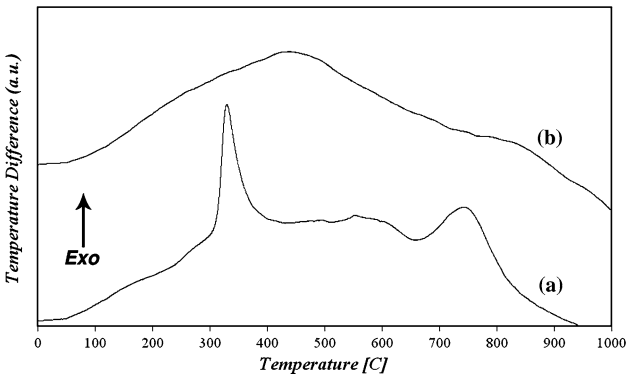

Fig. 10 DTA curves of Fe_2O_3 + 3Al + Fe (**a**) after 3 h and (**b**) after 20 h of milling times

exothermic and an endothermic peaks. The first exothermic peak (about 350 °C) is due to the reaction of elemental Fe and Al. The endothermic peak occurs at 670 °C, as a result of melting of remaining Al. The second exothermic peak around 750 °C represents the reaction between Al and Fe_2O_3. With an increase in the milling time, the DTA curve had no distinctive peaks, as the reaction among Fe, Al, and Fe_2O_3 has been completed after 20 h of ball milling. The broad DTA peak observed for sample milled for 20 h might be due to the ordering of Fe(Al) solid solution and grain growth.

Conclusions

Mechanical treatment behavior of 3Fe + Al and mechanochemical behavior of stoichiometric Fe_2O_3 + 2Al and $3Fe_2O_3$ + 8Al reactions, and off-stoichiometric Fe_2O_3 + 3Al + Fe reaction were studied during high-energy ball milling. The kinetics of these reactions accord well with that predicted by corresponding T_{ad} values. XRD patterns and cross-sectional images of powder particles revealed that the start time for reaction between Fe_2O_3 and Al is longer, as Fe is added to initial powder mixture, and the presence of pure Fe changed the modality of mechanochemical process from sudden to gradual reaction. The Fe_3Al intermetallic compound obtained during ball milling of 3Fe + Al and mechanochemical reaction of Fe_2O_3 + 3Al + Fe powder mixtures had a nanocrystalline structure with a crystallite size of 37 and 28 nm respectively. The particles of Fe_3Al and Fe_3Al-30 vol.%. Al_2O_3 were irregular in shape and the presence of in situ formed alumina led to a decrease in the crystallite and particle size. DTA studied showed the reaction among Fe_2O_3, Fe and Al was completed during ball milling.

References

1. Sauthoff G (1995) In: Intermetallics. VCH, Germany, p 86
2. Stollof NS (1998) Mater Sci Eng A258:1
3. Judkins RR, Roa US (2000) Intermetallics 8:1347
4. Stollof NS, Liu CT, Deevi SC (2000) Intermetallics 8:1313
5. Morris DG (1998) Intermetallics 6:753
6. Venugopal T, Roa KP, Murty BS (2005) Mater Sci Eng A393:382
7. Li J, Li F, Hu K (2004) J Mater Process Tech 147:236
8. Oleszak D (2004) J Mater Sci 39:5169
9. Oleszak D, Krasnowski M (2001) Mater Sci Forum 360–362:235
10. Matteazzi P, Caer GL, Mocellin A (1997) Ceram Int 23:39
11. Williamson GK, Hall WH (1953) Acta Metall 1:22
12. Fan RH, Sun JT, Gong HY, Sun KN, Wang WM (2005) Powder Tech 149:121
13. Enayati MH, Salehi M (2005) J Mater Sci 40:3933
14. Matteazzi P, Caer GL (1992) J Am Ceram Soc 75:2749
15. Nasu T, Tokumitsu K, Miyazawa K, Greer AL, Suzuki K (1999) Mater Sci Forum 312–314:185
16. El-Eskandarany MS, El-Bahnasawy HN, Ahmed HA, Eissa NA (2001) J Alloys Compd 314:286
17. Tokumitsu K, Nasu T, Suzuki K, Greer AL (1998) Mater Sci Forum 269–272:181
18. Nasu T, Tokumitsu K, Konno T, Suzuki K (2000) Mater Sci Forum 343–346:435
19. Dodd AC (2005) In: Lee B, Komarneni S (eds) Chemical processing of ceramics, 2nd edn. Taylor and Francis, p 65–75
20. Benjamin JS (1970) Metall Trans 1:2943
21. Munir ZA (1988) Ceram Bull 67:342
22. Schaffer GB, McCormick PG (1990) Metall Trans 21A:2789
23. Fan RH, Lu HL, Sun KN, Wang WX, Yi XB (2006) Thermochim Acta 440:129
24. Leonard RT, Koch CC (1997) Scripta Mater 36:36–41
25. Cullity BD (1969) In: Elements of X-ray diffraction. Addison-Welsey, Reading, MA, p 512